Statistical optimization of hydrogen production from bio-methanol steam reforming over Ni-Cu/Al_2O_3 catalysts

Yi-Kai Chih [1], Wei-Hsin Chen [1,2,3,*], Siming You [4], Chun-Han Hsu [5], Hong-Ping Lin [6], Salman Raza Naqvi [7], Veeramuthu Ashokkumar [8]

1. Department of Aeronautics and Astronautics, National Cheng Kung University, Tainan 701, Taiwan
2. Research Center for Smart Sustainable Circular Economy, Tunghai University, Taichung 407, Taiwan
3. Department of Mechanical Engineering, National Chin-Yi University of Technology, Taichung 411, Taiwan
4. James Watt School of Engineering, University of Glasgow, Glasgow, G12 8QQ, UK
5. National Tainan Junior College of Nursing, Tainan 700, Taiwan
6. Department of Chemistry, National Cheng-Kung University, Tainan 70101, Taiwan
7. School of Chemical and Materials Engineering (SCME), National University of Sciences and Technology, H-12, Islamabad 44000, Pakistan
8. Center of Excellence on Petrochemical and Materials Technology (PETROMAT), Chulalongkorn University, Pathumwan, Bangkok 10330, Thailand

*Corresponding author; E-mail: weihsinchen@gmail.com; chenwh@mail.ncku.edu.tw

Abstract

Hydrogen has emerged its importance for decarbonization to approach net-zero emissions in 2050. This study aims to develop three highly-porous Ni-Cu/Al_2O_3 catalysts (Ni-to-Cu weight ratio=10%, 20%, and 30%) for hydrogen production from the steam reforming of "Green" methanol (or bio-methanol). The prepared catalysts require no organic templates, thereby efficiently reducing unnecessary costs. With Taguchi orthogonal array design and analysis of variance (ANOVA), the impacts of selected operating factors on hydrogen productivity under ultrasonic sprays are investigated. The results reveal that the carrier gas flow rate is the most influential factor in H_2 yield at the steam-to-methanol molar ratio (S/C) of 1.5, whereas the temperature is the most impactful factor at S/C=2.0. The regression between the Taguchi effect value and the ANOVA F value develops a strong linear relationship. The optimal experimental conditions of Ni-Cu(30%)/Al_2O_3, reaction temperature of 300 °C, N_2 flow rate of 1,000 mL·min^{-1}, and S/C=2.0, achieve 100% methanol conversion, 39.74 vol% H_2 concentration in the product gas, and 2.93 mol·(mol CH_3OH)$^{-1}$ H_2 yield. Thes data also show superior performance compared to

those in the literature. In long-term stability tests, the prepared catalysts also exhibit high stability and effectiveness commensurate with commercialized Cu-based catalysts.

***Keywords*:** Hydrogen production; Methanol steam reforming (MSR); Non-noble metal; Cu-based catalyst; Taguchi method and analysis of variance (ANOVA); Optimization and statistics.

1. Introduction

In light of the ever more pressuring energy demand and environmental challenges, the connection between energy production and environmental sustainability has become a focal point in scientific research. One of the major factors responsible for global climate change is carbon dioxide emissions resulting from extracting energy out of fossil fuels through combustion [1-3]. To help mitigate carbon emissions, many efforts have been put into devising alternative energy production and storage methods based on renewable non-fossil fuels. Hydrogen, which almost has no emissions but water upon combustion, is considered a vital source of clean energy [4, 5] and an essential route to achieve net zero carbon emissions by 2050.

At present, there are four main approaches for hydrogen production [6]: (1) thermochemical methods such as natural gas reforming [7], coal gasification [8], and biomass gasification [9]; (2) electrochemical methods [10] such as water electrolysis from solar or wind power; (3) photocatalysis [11] for water splitting; and (4) biological methods for biohydrogen production. Among these approaches, thermochemical methods are of tremendous potential for large-scale, commercialized production, owing much to their high overall thermal-to-hydrogen efficiency ($\eta \sim$ 52%) and low production cost [12]. Hydrogen as one of the future energy carriers seems to be promising for fuel cell and hydrogen combustion vehicles, not only because of its environmental sustainability but also its high energy density (120 $MJ \cdot kg^{-1}$), which is about three times higher than that of gasoline [13].

Conventionally, around 96% of the world's hydrogen production by thermochemical methods has employed methane as the primary reactant [14]. Nevertheless, methanol provides a logistically easier and safer alternative for storing hydrogen. Methanol is a liquid transportation fuel that can be produced from fossil or renewable resources [15]. "Green" methanol (or bio-methanol) can be produced *via* biological (anaerobic digestion) [16], electrofuel (power-to-gas) [17], or

thermochemical (gasification) pathways [18]. Through thermochemical processes, bio-methanol can be produced from a variety of carbon-based feedstocks such as biomass. In such processes, biomass is subjected to high temperatures and pressures to produce a synthesis gas (syngas), which is then made to react with CO and H_2 at a high temperature and pressure to produce methanol [19].

Hydrogen can be extracted from bio-methanol at a low temperature *via* methanol steam reforming (MSR), where only a little CO is produced. Methanol has low-energy chemical bonds because of no C-C chemical bond [20]. Therefore, methanol steam reforming technology is very popular in the development of fuel processing for fuel cells and power generation [21, 22]. This is the reason why methanol is considered one of the major hydrogen-producing liquid fuels [23].

MSR, **Eq. (1)**, is a promising method for hydrogen production [24], owing much to its chemical efficiency. While MSR proceeds for hydrogen production, the side reactions of methanol decomposition (MD) [25], **Eq. (2)**, and water-gas shift reaction (WGSR) [26], **Eq. (3)**, also occur. The three reactions are given as follows:

$$CH_3OH + H_2O \rightleftharpoons 3H_2 + CO_2 \qquad \Delta H^0_{298} = 49.5\ kJ{\cdot}mol^{-1} \qquad (1)$$

$$CH_3OH \rightleftharpoons 2H_2 + CO \qquad \Delta H^0_{298} = 90.1\ kJ{\cdot}mol^{-1} \qquad (2)$$

$$H_2O + CO \rightleftharpoons CO_2 + H_2 \qquad \Delta H^0_{298} = -41.2\ kJ{\cdot}mol^{-1} \qquad (3)$$

Although triggering the MSR reaction requires heat input, it occurs at relatively low temperatures (200~300 °C) [27] compared to other commonly used methods such as the steam reforming of ethanol and methane, whose reaction temperatures exceed 600 °C and 800 °C, respectively [28]. Therefore, MSR has been a widely adopted method for hydrogen production.

As demonstrated in **Fig. S1** (supplementary materials), research on hydrogen production through methanol steam reforming (MSR) has risen over the past two decades. The growing interest in such a method reflects advancements in hydrogen production research, which relies on the high-performance catalyst. Sa et al. [20] reviewed the performance of various metallic catalysts

for methanol steam reforming (MSR) and summarized recent developments of copper-based catalysts in combination with metals in groups VIII through X. Xu et al. [29] compared the effects of catalyzing MSR with Cu-based and Pd-based catalysts over a ZnO-made supporter and found Pd/ZnO delivered higher CO_2 selectivity, which is an indicator of active MSR reaction. A more effective catalyst such as Pd is considerably less available and less affordable as a rare noble metal. Instead, the performance of Cu/ZnO at catalyzing MSR was found by Alejo et al. [30] to be satisfactory as well, with increased activity resulting from a synergy created in the process of forming a Cu-ZnO alloy. Palo et al. [31] discussed various catalysts, reactors, and MSR systems developments and identified the advantages and disadvantages of using methanol for hydrogen production.

As far as catalysts for MSR are concerned, combining Au-Ni and Au-Cu catalysts with carbon nanotubes supporters could enhance the catalysts' activity by increasing the contact surface between methanol and the catalysts [32]. In comparison, catalysts containing Ni exhibited higher selectivity to hydrogen than those without Ni at the same temperature. Moreover, the inclusion of Ni in catalysts helped suppress coke deposition and the undesired sintering of the active phases, which resulted in enhanced stability and hydrogen yield [33, 34]. These findings suggest that bimetallic alloys with Ni make effective catalysts in MSR processes. More accessible and inexpensive, Ni-Cu composites can replace noble metals as catalysts in hydrogen-producing processes. Ni-Cu catalysts have been adopted in several processes such as ethanol steam reforming [32], methane decomposition [33], methane steam reforming [34], methane dry reforming [35, 36], methanol partial oxidation [37], methanol decomposition [38], CO and CO_2 hydrogenation [39], and methanol steam reforming [40]. From the circular economy perspective, the reactants for producing Ni-Cu composites can be extracted from the wastewater of semiconductor manufacturing processes, facilitating waste material recycling [41].

Regardless of the choice of catalyzing materials, reactions can be expedited with improvements to the material feeding procedure. Practice in this respect is using ultrasonic sprays in industrial, medical, chemical, and agricultural research and applications [42-44]. Through ultrasonic vibration, droplets of various sizes are produced, with which the intensity and velocity of sprays can be controlled. In addition, ultrasonic sprayers can be easily installed on various production lines to help improve spray quality.

To further enhance efficiency, statistical methods are employed to identify the optimal combination of materials and other key factors. Two useful tools are the Taguchi method and the analysis of variance (ANOVA) [45]. The Taguchi method [46], based on an orthogonal array design, provides a tool to save time and expenses by limiting the number of experimental cases needed to produce statistically reliable outcomes, where the signal-to-noise ratio (S/N) analysis is utilized to help identify the optimal combination of factors [47]. ANOVA examines the sensitivity of response variables to variations of different input parameters [48]. It shows the contribution of controlled parameters in changing quality characteristics [49, 50]. When combining the Taguchi method with ANOVA, the S/N ratios from the Taguchi orthogonal array are input into ANOVA, which processes them using the contribution of parameters, F-ratio of parameters, the variance of parameters, the sum of squares of parameters, and degree of freedom [51]. ANOVA can be used complementary with the Taguchi method because Taguchi analysis shows the effect levels of those parameters on characteristics, and ANOVA represents the contribution of control parameters on quality characteristics.

In light of the above, catalyzing MSR with the highly-porous Ni-Cu/Al_2O_3 made without the use of organic templates, along with feeding reactants by ultrasonic sprays, seems to be a promising approach to producing hydrogen in a cost-efficient and environmentally friendly route. Under a design of experiment (DOE), the methanol conversion and H_2 yield levels from each case as

arranged following the Taguchi method will then be examined through the lens of S/N ratios in ANOVA. Guided by the insight provided by the aforementioned methods, this novel approach has the potential for high methanol-based hydrogen productivity with low costs and pollution.

2. Methodology

2.1. Preparation of Ni-Cu/Al_2O_3 catalysts

In this study, the Ni-Cu/Al_2O_3 catalysts were synthesized via a hydrothermal reconstructed method (**Fig. S2**) [35, 36]. 1.5 g of $Cu(NO_3)_2$ (1.5 g, Merck, >95%) and 0.196 g of $Ni(NO_3)_2$ (Merck, >95%) were dissolved in 100.0 mL water. 2.53 g of activated alumina (Merck, >95%) was dispersed in 80.0 mL of water. The copper/nickel solution and 2.0 M NaOH were added to the alumina solution. The pH value of the mixed gel solution was maintained at 9.0. After stirring for 2 h, the gel solution was hydrothermally treated at 70 °C for 24 h. The Ni-Cu/Al_2O_3 samples were then obtained by filtration and drying. In this work, the Ni-Cu/Al_2O_3 samples using 0.196 g, 0.392 g, and 0.588 g $Ni(NO_3)_2$. They lead to the Ni-to-Cu weight ratios of 1:10, 2:10, and 3:10, respectively. The three catalysts are denoted as Ni-Cu(10%)/Al_2O_3, Ni-Cu(20%)/Al_2O_3, and Ni-Cu(30%)/Al_2O_3 in this study.

2.2. Characteristics analysis of Ni-Cu/Al_2O_3 catalysts

To characterize the three catalysts, N_2 sorption measurements were operated in a surface area analyzer (Micromeritics TriStar II), where the Brunauer-Emmett-Teller (BET) method was used to calculate the catalysts' specific surface areas. The samples were degassed at 120 °C for 6 h. The X-ray diffraction (XRD) patterns of the catalysts were taken with an X-ray diffractometer (Rigaku MultiFlex) (40 kV, 20 mA), using Cu K_α radiation. Energy-dispersive X-ray spectroscopy (EDS, Gatan EDAX), ultra-high-resolution field-emission scanning electron microscope (SEM, using HITACHI SU-5000), and transmission electron microscope (TEM, using JEOL JEM-2100F) were

performed to ascertain the morphologies and actual compositions of the catalysts. It should be noted that the catalysts were coated with a layer of gold to enhance the quality of the surface scan in the SEM analysis. The catalysts' thermal characteristics were analyzed using a thermogravimetric analyzer (SDTQ600 TGA, TA Instruments). A sample with around 5 mg was loaded in an alumina pan and heated from 105 °C to 800 °C at a constant heating rate of 20 °C·min^{-1} where the oxygen flow rate was 100 mL·min^{-1}.

2.3. MSR reaction system

A fixed-bed reaction system (**Fig. 1)** was constructed to perform MSR. The prepared Ni-Cu/Al_2O_3 catalysts were placed in a quartz tube (30 mm i.d.). A layer of quartz fiber was behind the catalyst and at the tube's bottom to adjust the catalyst to an optimal location from the sprays. The quartz tube was then preheated to 200-300 °C with a heating tape (D98L-TIP80) wound around it. The tube and the tape were then wrapped in a layer of refractory ceramic fibers to prevent heat from evading. In the center of the catalyst bed tube, a K-type thermocouple was placed to measure the reaction temperature.

During the experiments, the flow rate of nitrogen (99.99%) was controlled by a mass flow controller (KD-4000) in conjunction with a controller readout (Brooks 5850E) which displayed the real-time flow rate. Prior to the measurements, the flow rate controller was calibrated by an air flow calibrator (Gillan-Stander Flow Cell-P / N 800266-1). At the same time, an HPLC pump (JASCO Model PU-2080-ND) pumped the methanol solution into the reactor through the ultrasonic spray nozzle. The solution was turned into fine droplets, so methanol and water could react with the catalysts at a higher reaction rate and thereby higher methanol conversion. The reaction products flew through a condenser (YIHDER, BL710) which cooled down the effluent and collected the condensed water. The condensed gas then passed through a drier filled with silicone gel to ensure they were thoroughly demoisturized. Lastly, the volumetric concentrations

of carbon dioxide, carbon monoxide, and methane were measured with a gas analyzer (GA, Fuji ZRJF5Y23-AERYR-YKLYYCY-A). To guarantee the experimental quality, the GA was calibrated by nitrogen (purity > 99.9%) and a standard gas (CO_2: 20.12 vol%; CO: 29.98 vol%, CH_4: 11,150 ppm; and N_2: balance). The gas chromatography (GC, SRI 310C TCD) was equipped with a thermal conductivity detector (TCD) and an auto-sampling system to measure the H_2 concentration**.** Five gas mixtures of H_2 and N_2 with various H_2 concentrations (i.e., 10, 20, 30, 40, and 50 vol%) were used to establish a calibration curve to measure the H_2 concentration in the product gas. Each experimental case lasted longer than 42 min to ensure that the reaction reached a steady state. The 18 cases were performed repeatedly, and the relative errors in gas concentrations, H_2 yield, and methanol conversion were controlled below 3.5%, ascertaining the reproducibility of the experiments.

2.4. Methanol conversion and H_2 yield

Based on the flow rate and CO, CO_2, and CH_4 concentrations, the methanol conversion can be calculated by the following equation:

$$CH_3OH\ conversion\ (\%) = \left(\frac{\dot{n}_{CO_2,out} + \dot{n}_{CO,out} + \dot{n}_{CH_4,out}}{\dot{n}_{CH_3OH,in}}\right) \times 100 \quad (4)$$

where $\dot{n}$ stands for the molar flow rate (mol·min^{-1}), and the subscripts "*in*" and "*out*" designate inflow and outflow, respectively. Meanwhile, the H_2 yield is identified according to the following equation:

$$H_2\ yield\ (mol\cdot(mol\ CH_3OH)^{-1}) = \left(\frac{\dot{n}_{H_2}}{\dot{n}_{CH_3OH}}\right) \quad (5)$$

2.5. Taguchi orthogonal array and ANOVA analysis

The Taguchi orthogonal array is an appropriate experimental design for determining the relative impact of a variety of factors on the phenomena of interest. By arranging chosen levels

representing different values of each factor in an orthogonal array, it is unnecessary to consider all possible parameter combinations [37]. The real values of the dependent variable are transformed into a "signal-to-noise" (S/N) ratio, a general conception aimed at measuring the experimental quality. The term "signal" refers to the desired real value of the independent variables, while "noise" refers to other factors that are unaccounted for [38]. Mathematically, the S/N ratio can be calculated with the following equation:

$$S/N\ ratio\ =\ -10\ log\ \left(\frac{1}{y^2}\right) \tag{6}$$

where *y* designates the measured value of the dependent variable.

Conceptually, the distribution of S/N ratios can be interpreted in light of the following types: the-nominal-the-better (NB), the-larger-the-better (LB), and the-smaller-the-better (SB) [39]. Since the objective of this study is to maximize methanol conversion or H_2 yield, the type chosen to interpret S/N ratios is the LB type, where a larger S/N ratio implies better performance or experimental quality. The optimal combination of operating conditions can be identified.

Three operating parameters, namely, the Ni-to-Cu weight ratio of the catalyst (Factor A), reaction temperature (Factor B), and the volume flow rate for N_2 as the carrier gas (Factor C), were selected in the designed orthogonal array of the Taguchi method. As shown in **Table 1**, the experiments were conducted with three reacting temperatures (200-300 °C), three Ni-to-Cu weight ratios (10-30%), and three N_2 flow rates (1,000-2,000 $mL \cdot min^{-1}$). Based on the control factors and parameter levels specified above, an L9 (3^3) orthogonal array was developed, where nine sets of experiments were carried out. An additional factor, the steam-to-carbon (or steam-to-methanol) molar ratio (S/C), was used as a control variable. Two S/C values of 1.5 and 2.0 were chosen to highlight the variable's impact on the outcome. Accordingly, a total of 18 cases were organized

into two clusters with Cases 1-9 (where S/C=1.5) reported in **Table 2a** and Cases 10-18 (where S/C=2.0) in **Table 2b.**

Although the Taguchi orthogonal array can provide the sensitivity analysis of factors, it could not recognize the impact of test errors. To make necessary statistical corrections by separating the effects of experimental noise from the true impact of explanatory factors on the experimental results, the analysis of variance (ANOVA) was also used [40, 41]. In ANOVA, the sum of squares of deviation (S_i) is defined as

$$S_i = 3 \times \sum_{j=1}^{3} (K_{ij} - \overline{y})^2 \quad (7)$$

where K_{ij} is the true value of the dependent variable from each case with i referring to a given factor symbol (A/B/C/D) and j referring to a given level number (1/2/3); $\bar{y}$ is the mean value of the dependent variable in all cases. The formula for the ANOVA F-test statistic is defined as

$$F = \frac{Sum\ of\ square\ of\ conversion/f}{Sum\ of\ square\ of\ error/\ f_e} = \frac{S_i/f}{S_f/[(N-1)-f]} \quad (8)$$

where the degree of freedom for every factor f is the number of every factor's level -1, f_e is determined as (N-1)-f, and N is the total number of tests. Since all the columns in orthogonal design are occupied by factors, the sum of squares of deviation for error S_f can be represented by the minimum value of those for all factors. By comparing F of every factor with its critical value under different reliabilities, the significance of every factor can be identified [42].

2.6. Long-term stability test

The decline of H_2 concentration in the reaction process is an important indicator of the stability of catalyzing materials used in a hydrogen-producing process. To gauge the long-term stability of different catalysts, Ni-Cu(10%)/Al_2O_3 and Ni-Cu(30%)/Al_2O_3 were selected for longer-term tests conducted along with a Cu-based oxidant (Apex Green Technology Co., Ltd.) that had wide

commercial applications. The H_2 concentration with sampling for GC analysis was measured per 15 min throughout the experiment.

3. Results and discussion

3.1. Characterization of Ni-Cu/Al_2O_3 catalysts with different Ni contents

According to Lin et al. [35, 36], Ni-Cu/Al_2O_3 compounds can be created through the interaction of metal ions and Al_2O_3 in an alkali environment around pH 9.0. After three hours of sintering at 600 °C, these compounds can be turned into metal oxidants that are suitable to catalyze MSR. The structures of the resultant Ni-Cu/Al_2O_3 are analyzed with BET, XRD, and SEM instruments. With different amounts of Ni, the catalysts Ni-Cu(10%)/Al_2O_3, Ni-Cu(20%)/Al_2O_3, and Ni-Cu(30%)/Al_2O_3, have surface areas of 170, 158, and 136 $m^2 \cdot g^{-1}$, respectively, according to the BET. As shown in **Fig. 2a**, type IV isothermal curves indicate a mesoporous structure [43]. These results suggest that porous Ni-Cu/Al_2O_3 catalysts are made without organic templates.

In terms of crystal patterns, the X-ray diffraction patterns of the catalysts are illustrated in **Fig. 2b**, where two of the sintering process's main products, $CuAl_2O_4$ and CuO, are present [44]. The presence of $CuAl_2O_4$ phases (JCPDS No. 01 -078-1605) will result in the peaks at 36.7°, 44.7°, and 65.0 °. **Fig. 2b** clearly presents the peaking pattern of $CuAl_2O_4$ in the three catalysts, with a less evident presence of CuO (JCPDS No. 45-0937), whose phases should peak at 35.4° and 38.7° [45]. Overall, the broad and "weak" (low-intensity) diffraction peaks indicate high degrees of dispersion among the Cu oxidants' particles. On the other hand, the Ni is homogeneously bonded to the Cu/Al_2O_3 structure without forming its crystals (**Fig. 2b**). The situation remains unchanged with the addition of greater amounts of Ni (i.e., from 10% to 30%) to the catalysts.

Fig. 3 shows the SEM images of Ni-Cu (10%)/Al_2O_3 with magnifications of 2,000 (**Fig. 3a**) and 20,000 (**Fig. 3b**). The Ni-Cu (10%)/Al_2O_3 particles appear to cluster into flakes with sizes

exceeding 2 μm (**Fig. 3a**), as a result of filtering and squeezing. With a magnification factor of 20,000, it is clear that the surfaces of Ni-Cu (10%)/Al_2O_3 clusters are full of needle-shaped structures with a length of approximately 100-200 nm **(Fig. 3b)**. Such a morphology reflects a high total surface area which is conducive to a more speedy reaction.

3.2. Gas production and reaction performance

Eighteen experimental cases are conducted based on the Taguchi orthogonal array in **Table 2**. As shown in **Tables 2a** and **2b**, Cases 1-9 are performed at the condition of S/C=1.5, while Cases 10-18 are conducted at S/C=2.0. The product gas's resultant H_2, CO_2, CO, and CH_4 concentrations are presented in radar char and shown in **Figs. 4** and **5**. Overall, the H_2 concentration ranges from 16.43 to 39.74 vol% (**Figs. 4a-b**), accounting for the highest concentration among the four gases. Cases 1, 6, and 8 at S/C=1.5 demonstrate high levels of H_2 concentration (> 37 vol%) (**Fig. 4a**). In contrast, lower H_2 concentrations are exhibited in Cases 3 and 7 (24.22-24.57 vol%. As shown in **Table 2**, the high H_2 concentrations are positively associated with a low carrier gas flow rate (1,000 $mL \cdot min^{-1}$). A lower carrier gas flow rate leads to a longer retention time and a relatively higher concentration of the reactants, thereby resulting in higher methanol conversion and H_2 concentration. Another major factor determining the reaction performance is reaction temperature, which is also positively associated with H_2 concentration. Detailed phenomena will be discussed in greater detail in section 3.3.

A similar pattern in the radar char at S/C=2.0 can be found in **Fig. 4b**. A comparison between **Figs. 4a** and **4b**, the cases with the lowest H_2 concentrations at S/C=2.0, namely, Cases 12 and 16, show even lower levels of H_2 concentration than those of Cases 3 and 7, the poorest performing cases at S/C=1.5. These results suggest that increasing the water-to-methanol molar ratio from 1.5 to 2.0 lowers hydrogen productivity. Thermodynamically, a higher S/C ratio is conducive to

methanol conversion. However, a relatively higher amount of water to methanol added to the reactor will consume more energy for its latent heat, thereby suppressing hydrogen production.

Eqs. (2) and **(3)** indicate that CO in MSR comes from methanol decomposition (MD) and water gas shift reaction (WGSR). Le Chartilier's principle states that a high temperature facilitates MD, whereas a low temperature favors WGSR [46]. This implies, in turn, that a high temperature intensifies CO formation, whereas a low temperature is conducive to CO consumption. The CO concentration shown in **Fig. 4c** is in the range of 0-5.2 vol%, with Cases 4, 5, 7, and 8 giving higher CO concentrations. On the other hand, Cases 3, 6, and 9 give rise to lower CO concentrations. Comparative analysis reveals that the CO concentration is higher when the reaction temperature is 250 or 300 °C, whereas the lower CO concentration develops at 200 °C. Since the outcomes in **Fig. 4c** are aligned with Le Chartilier's principle, MD and WGSR are also involved in H_2 production. The entire radar chart in **Fig. 4d** is similar to **Fig. 4c**, where Cases 12, 15, and 18 demonstrate lower CO concentrations under S/C=2.0. This further confirms that MD is a crucial reaction for CO production.

Eqs. (1) and **(3)** indicate that the higher the CO_2 concentration, the higher the H_2 production. The CO_2 concentrations from the 18 cases at S/C=1.5 and 2.0 are displayed in **Figs. 5a-d**, where the concentration ranges from 4.80 to 12.04 vol%. Overall, the CO_2 concentrations are higher than the CO concentrations, which is conducive to H_2 formation. Cases 1, 6, and 8 demonstrate higher CO_2 concentrations; this conforms with the H_2 concentrations in **Fig. 4a**. In theory, higher reaction temperatures lead to higher CO_2 concentrations. Yet, Case 1, carried out at 250 °C, did not pose a higher CO_2 concentration than Case 6, performed at 200 °C. This suggests that the higher amount of Ni in the catalyst employed in the latter (20%) helps induce CO_2-producing reactions (**Eqs. (1)** and **(3)**).

In addition to H_2, CO_2, and CO, CH_4 is also detected in the gas product. This is unsurprising since Ni-based catalysts are commonly used to induce methanation from syngas [47]. The involved methanation reactions are expressed as follows [48]:

$$CO + 3H_2 \rightleftharpoons CH_4 + H_2O \qquad \Delta H_{298}^0 = -205.8\ \text{kJ·mol}^{-1} \tag{9}$$

$$CO_2 + 4H_2 \rightleftharpoons CH_4 + 2H_2O \qquad \Delta H_{298}^0 = -165.0\ \text{kJ·mol}^{-1} \tag{10}$$

The CH_4 concentration is below 1,000 ppm in most cases, significantly lower than CO_2, CO, and H_2, as shown in **Figs. 5c** and **5d**. The highest CH_4 concentration occurs in Case 8 with 3,766 ppm at the highest reaction temperature of 300 °C and the lowest carrier gas flow rate of 1,000 $mL·min^{-1}$. Thermodynamically, a high temperature disadvantages CH_4 formation. It follows that the reaction temperature plays a minor effect on CH_4 formation. Cases 8 and 17 lead to higher H_2, CO_2, and CO concentrations, facilitating CH_4 formation, especially under a low flow rate. This is the primary reason causing high CH_4 formation. Like the three gases mentioned above, the profile of CH_4 at S/C=2.0 (**Fig. 5d**) is similar to that at S/C=1.5 (**Fig. 5c**).

Based on the measured CO_2, CO, and CH_4 concentrations, the methanol conversion radar chars at S/C=1.5 and 2.0 are displayed in **Fig. 6,** where the conversion is calculated by **Eq. (4)**. With the operating condition of S/C=1.5, **Fig. 6a** depicts that methanol conversion ranges from 59.33% to 100%. Cases 5, 7, and 8 pose a conversion above 90%, corresponding to a high reaction temperature of 300 °C and a low carrier gas flow rate of 1,000 $mL·min^{-1}$. The highest conversion (100%) achieves in Case 8, resulting from the operation of a higher reaction temperature (250 °C) along with a greater Ni content (30%). **Fig. 6b** with S/C=2.0 depicts that more cases (i.e., Cases 10, 13, 14, 16, and 17) can achieve high methanol conversion (> 90%), where these cases are triggered at temperatures no less than 250 °C. Accordingly, **Figs. 6a** and **6b** suggest that a higher S/C ratio is conducive to H_2 production since increased H_2O supply enables methanol to react more thoroughly along the paths of **Eqs. (1)** and **(3)**.

The radar chars of the H_2 yield, calculated according to **Eq. (5)**, at S/C=1.5 and 2.0 are shown in **Fig. 7**. From **Eq. (1)**, the theoretical highest H_2 yield is 3 mol·(mol CH_3OH)$^{-1}$ if methanol is wholly converted and no other side gases (e.g., CO and CH_4) are produced. **Fig. 7a** with S/C=1.5 shows that Cases 1, 5, and 8 render higher H_2 yields of 2.52, 2.75, and 2.93 mol·(mol CH_3OH)$^{-1}$, respectively. In these cases, their reaction temperatures are 250 °C or above. In **Fig. 7b** with S/C=2.0, the higher H_2 yields develop in Cases 10, 14, and 17, corresponding to 2.72, 2.88, and 2.77 mol·(mol CH_3OH)$^{-1}$, respectively. The three cases tally with the results in **Fig. 7a.** In comparing the H_2 yield in the two figures, the entire trend in **Fig. 7a** coincides with that in **Fig. 7b**. All the experimental parameters and MSR results are reported in **Table 3**.

3.3. Taguchi method and ANOVA analysis

The S/N ratios of H_2 yield across all 18 cases were calculated by **Eq. (6)** and reported in **Fig. 8** and **Table 4**. The higher the S/N ratio, the higher the H_2 yield, so the S/N ratio can serve as an indicator of MSR performance. Align with the radar charts in **Fig. 7**, Cases 8 (S/N=9.34) and 14 (S/N=9.19) stand out as having the most significant levels of H_2 yield at S/C=1.5 and 2.0, respectively. In ANOVA analysis, the F value indicates a factor's impact on the outcome, where a high F value stands for a significant impact [49]. For ANOVA at a confidence interval of 95% using S_i and S_f values derived from **Eqs. (7)** and **(8)**, F values for the three factors' relative influences on the H_2 yield are listed in **Table 5**, where **Table 5a** reports the results from Cases 1-9 (S/C=1.5) and **Table 5b** reports the results from Cases 10-18 (S/C=2.0).

Table 5a at S/C=1.5 indicates that Factor C (i.e., the carrier gas flow rate) has the highest F value (50.25) among the three factors, implying that a longer retention time allows more completed reaction. On the other hand, **Table 5b** at S/C=2.0 reveals that Factor B (i.e., reaction temperature) has the highest F value (21.38), suggesting that a greater supply of H_2O in the reaction more replies to the heat provided [50]. Overall, the results of ANOVA analysis suggest the same ranking order

among the three factors across the two groups of cases as the Taguchi method's results. To confirm this observation, linear regressions at S/C=1.5 and 2.0 are performed and shown in **Figs. 9a** and **9b**, respectively. The regressions show strongly linear distributions (R^2=0.9718 at S/C=1.5 and R^2=0.9827 at S/C=2.0). Accordingly, it should be concluded that the Taguchi method conforms with ANOVA, showing the analysis reliability.

3.4. Recycling of Ni-Cu/Al_2O_3 catalysts

Fig. 10 presents the thermogravimetric analysis (TGA) curves of used Ni-Cu/Al_2O_3 catalysts to analyze their coking characteristics where the heating temperatures are in the range of 105°C up to 775°C. These curves reveal that the weight loss of the Ni-Cu/Al_2O_3 catalysts, namely, 10%, 20%, and 30%, was less than 5%. Derivative thermogravimetric (DTG) analysis indicates that the weight loss mainly occurred between 105°C and 300°C, reflecting that the coke on the surfaces of the catalysts was mostly due to the low molecular weight organic compounds. As a consequence, it is concluded that the prepared Ni-Cu/Al_2O_3 catalysts are thermally stable and coke-resistance [51].

The used catalysts are regenerated through calcination to 600 °C for coke removal to evaluate the potential of reusing the Ni-Cu/Al_2O_3 catalysts. **Fig. 11a** shows the N_2 sorption isotherms of the recycled Ni-Cu/Al_2O_3 catalyst. All the catalysts display type IV isotherms and undergo capillary condensation of P/P_0 values in the range of 0.4-0.9 [52, 53]. The recycled Ni-Cu/Al_2O_3 catalysts with Ni contents of 10%, 20%, and 30% have surface areas of 123, 118, and 129 $m^2 \cdot g^{-1}$, respectively. These results show that all the recycled Ni-Cu/Al_2O_3 catalysts remain in high surface areas and keep a typical mesoporous structure after calcination. It is inferred that the Ni-Cu/Al_2O_3 catalysts obtained using the proposed synthesis route have good thermal stability and can be regenerated by coke removal via calcination. **Fig. 11b** shows the XRD patterns of the recycled Ni-Cu/Al_2O_3 catalysts. All of the patterns contain broad and weak diffraction peaks, indicating an amorphous structure. However, the diffraction peaks of CuO gradually become sharper only for the 10% Ni-

add sample, which suggests adding Ni improves the dispersion of the metal species and produces a synergistic effect between the Ni and Cu in the Ni-Cu/Al_2O_3 structure.

3.5. Long-term stability test and performance comparison

Fig. 12 demonstrates the long-term stability test of three catalysts (i.e., Ni-Cu(10%)/Al_2O_3, Ni-Cu(30%)/Al_2O_3, and a commercial Cu-based catalyst) in terms of hydrogen concentration. The H_2 concentration resulting from each experimental case is normalized based on its maximum concentration during the test. In the three tests for 24 h, the operating conditions are S/C=2.0, carrier gas flow rate=1,000 $mL \cdot min^{-1}$, and a reaction temperature of 250°C. All three systems denoted consistent results beyond the initial 24 hours, which suggests that the hydrogen-producing capacity of both variants of the Ni-Cu/Al_2O_3 catalysts is as stable as that of the commercialized catalyst.

3.6. Comparison of the present study to other works

Table 6 compares the performance of the prepared catalysts in this study and those from other works in the literature. Catalysts with different ingredients may work to different effects in association with the same supporting material. The significant difference in methanol conversion achieved by Cu/MCM-41 and Ni/MCM-41 suggests that the use of Cu is conducive to methanol-to-hydrogen conversion due to the highly active nature of the metal [54]. Cu has been used in combination with other metals such as Zn, In, Ce to form catalyzing alloys, while the oxidants of Si, Zr, SBA or Al have been employed to serve as supporting materials [55-60]. In these studies within a temperature interval of 220-320°C, the methanol conversion ranged from 63.5% to 99.3%. Alternatively, Ni-Cu catalysts working in a temperature interval of 200-300°C resulted in a wide range of methanol conversion (5-100%) and hydrogen yield (1.2-2.08 $mol \cdot (mol\ CH_3OH)^{-1}$) [61-66]. In contrast, the Ni-Cu catalysts in the present study attain complete methanol conversion

(100%) along with the highest hydrogen yield of 2.93 mol·(mol CH_3OH)$^{-1}$ at 300°C, showing the excellent performance of the prepared Ni-Cu catalysts.

4. Conclusions

This study has successfully prepared three Ni-Cu-based catalysts for high-performance methanol steam reforming to produce hydrogen under ultrasonic sprays. The Taguchi method and analysis of variance (ANOVA) have also been successfully employed to analyze hydrogen production. The XRD and BET analyses reveal that the prepared Ni-Cu/Al_2O_3 catalysts mainly comprise an amorphous structure with a specific surface area of up to 170 $m^2 \cdot g^{-1}$. Distinct from past studies where catalysts typically exhibited a multi-spherical morphology, the prepared catalysts are featured by a unique acicular morphology from SEM observations. Considering three factors of catalyst type, reaction temperature, and carrier gas (N_2) flow rate at two different steam-to-methanol ratios (S/C=1.5 and 2.0), the Taguchi and ANOVA analyses suggest that the N_2 flow rate is the most influential parameter on the H_2 yield at S/C=1.5, whereas it is the reaction temperature at S/C=2,0. These results reveal that the water supply in the feedstock will alter the reaction characteristics. The Taguchi's effect value and the ANOVA's F value exhibit a strong linear relationship ($R^2 > 0.97$) in the regression analysis, elucidating the analysis's reliability. The analysis suggests the optimal conditions occurring at Ni-Cu(30%)/Al_2O_3, 300 °C reaction temperature, 1,000 mL·min^{-1} N_2 flow rate, and 2.0 S/C ratio, achieving 100% methanol conversion, 39.74% hydrogen concentration, and 2.93 mol·(mol CH_3OH)$^{-1}$ H_2 yield. These results show superior performance to the data reported in the literature. Moreover, the catalyst durability tests show the high stability and effectiveness of the prepared catalysts. These outcomes suggest that the developed catalysts, devices, and operating conditions provide a promising technology for

achieving high-performance hydrogen production from MSR, which is conducive to clean fuel production and approaching the net zero target.

Acknowledgments

The authors would like to acknowledge the financial support of the Ministry of Science and Technology, Taiwan, R.O.C., under the grant numbers MOST 108-2221-E-006-127-MY3 and MOST 110-2622-E-006-001-CC1 for this research. The authors also gratefully acknowledge the the use of EM000700, EM000800, XRD005100 of 110-2731-M-006-001 belonging to the Core Facility Center of National Cheng Kung University (NCKU), Taiwan.

References

[1] Wuebbles DJ, Jain AK. Concerns about climate change and the role of fossil fuel use. Fuel Processing Technology 2001;71(1):99-119.

[2] Lazarus M, van Asselt H. Fossil fuel supply and climate policy: exploring the road less taken. Climatic Change 2018;150(1):1-13.

[3] Johnsson F, Kjärstad J, Rootzén J. The threat to climate change mitigation posed by the abundance of fossil fuels. Climate Policy 2019;19(2):258-74.

[4] Ji Y, Xie J, Yang Y, Fu X, Sun R, Wong C. NiCoP 1D nanothorns grown on 3D hierarchically porous Ni films for high performance hydrogen evolution reaction. Chinese Chemical Letters 2020;31(3):855-8.

[5] Wang Y, He F, Chen L, Shang J, Wang J, Wang S, et al. Acidification and bubble template derived porous g-C3N4 for efficient photodegradation and hydrogen evolution. Chinese Chemical Letters 2020;31(10):2668-72.

[6] Satyapal S, Petrovic J, Read C, Thomas G, Ordaz G. The U.S. Department of Energy's National Hydrogen Storage Project: Progress towards meeting hydrogen-powered vehicle requirements. Catalysis Today 2007;120(3):246-56.

[7] Pakhare D, Spivey J. A review of dry (CO2) reforming of methane over noble metal catalysts. Chemical Society Reviews 2014;43(22):7813-37.

[8] Ding L, Zhou Z, Guo Q, Huo W, Yu G. Catalytic effects of Na2CO3 additive on coal pyrolysis and gasification. Fuel 2015;142:134-44.

[9] Wu Z, Li Y, Xu D, Meng H. Co-pyrolysis of lignocellulosic biomass with low-quality coal: Optimal design and synergistic effect from gaseous products distribution. Fuel 2019;236:43-54.

[10] Xu D, Zhang Y, Hsieh T-L, Guo M, Qin L, Chung C, et al. A novel chemical looping partial oxidation process for thermochemical conversion of biomass to syngas. Appl Energy 2018;222:119-31.

[11] Shaner MR, Atwater HA, Lewis NS, McFarland EW. A comparative technoeconomic analysis of renewable hydrogen production using solar energy. Energy Environ Sci 2016;9(7):2354-71.

[12] Balat M. Thermochemical Routes for Biomass-based Hydrogen Production. Energy Sources, Part A: Recovery, Utilization, and Environmental Effects 2010;32(15):1388-98.

[13] Byun M, Lee B, Lee H, Jung S, Ji H, Lim H. Techno-economic and environmental assessment of methanol steam reforming for H2 production at various scales. International Journal of Hydrogen Energy 2020;45(46):24146-58.

[14] Nikolaidis P, Poullikkas A. A comparative overview of hydrogen production processes. Renewable and Sustainable Energy Reviews 2017;67:597-611.

[15] Arnaiz del Pozo C, Cloete S, Jiménez Álvaro Á. Techno-economic assessment of long-term methanol production from natural gas and renewables. Energy Conversion and Management 2022;266:115785.

[16] Patel SKS, Gupta RK, Kalia VC, Lee J-K. Integrating anaerobic digestion of potato peels to methanol production by methanotrophs immobilized on banana leaves. Bioresource Technology 2021;323:124550.

[17] Ababneh H, Hameed BH. Electrofuels as emerging new green alternative fuel: A review of recent literature. Energy Conversion and Management 2022;254:115213.

[18] Larose S, Labrecque R, Mangin P. Electrifying with High-Temperature Water Electrolysis to Produce Syngas from Wood via Oxy-Gasification, Leading to Superior Carbon Conversion Yield for Methanol Synthesis. Applied Sciences 2021;11(6):2672.

[19] Zang G, Sun P, Elgowainy A, Wang M. Technoeconomic and Life Cycle Analysis of Synthetic Methanol Production from Hydrogen and Industrial Byproduct CO2. Environmental Science & Technology 2021;55(8):5248-57.

[20] Sá S, Silva H, Brandão L, Sousa JM, Mendes A. Catalysts for methanol steam reforming—A review. Applied Catalysis B: Environmental 2010;99(1):43-57.

[21] Gkanas EI, Khzouz M, Panagakos G, Statheros T, Mihalakakou G, Siasos GI, et al. Hydrogenation behavior in rectangular metal hydride tanks under effective heat management processes for green building applications. Energy 2018;142:518-30.

[22] Xing S, Zhao C, Ban S, Su H, Chen M, Wang H. A hybrid fuel cell system integrated with methanol steam reformer and methanation reactor. International Journal of Hydrogen Energy 2021;46(2):2565-76.

[23] Holladay JD, Wainright JS, Jones EO, Gano SR. Power generation using a mesoscale fuel cell integrated with a microscale fuel processor. Journal of Power Sources 2004;130(1):111-8.

[24] Iulianelli A, Ribeirinha P, Mendes A, Basile A. Methanol steam reforming for hydrogen generation via conventional and membrane reactors: A review. Renewable and Sustainable Energy Reviews 2014;29:355-68.

[25] Garcia G, Arriola E, Chen W-H, De Luna MD. A comprehensive review of hydrogen production from methanol thermochemical conversion for sustainability. Energy 2021;217:119384.

[26] Chen W-H, Chen C-Y. Water gas shift reaction for hydrogen production and carbon dioxide capture: A review. Applied Energy 2020;258:114078.

[27] Chein R-Y, Chen Y-C, Lin Y-S, Chung JN. Hydrogen production using integrated methanol-steam reforming reactor with various reformer designs for PEM fuel cells. International Journal of Energy Research 2012;36(4):466-76.

[28] Basile A, Iulianelli A, Longo T, Liguori S, De Falco M. Pd-based Selective Membrane State-of-the-Art. In: De De Falco M, Marrelli L, Iaquaniello G, editors. Membrane Reactors for Hydrogen Production Processes. London: Springer London; 2011, p. 21-55.

[29] Xu X. Generalization of the Sherman–Morrison–Woodbury formula involving the Schur complement. Applied Mathematics and Computation 2017;309:183-91.

[30] Rosen M. Environmental sustainability tools in the biofuel industry. Biofuel Research Journal 2018;5:751-2.
[31] Palo DR, Dagle RA, Holladay JD. Methanol Steam Reforming for Hydrogen Production. Chemical Reviews 2007;107(10):3992-4021.
[32] Mierczynski P, Vasilev K, Mierczynska A, Maniukiewicz W, Szynkowska MI, Maniecki TP. Bimetallic Au–Cu, Au–Ni catalysts supported on MWCNTs for oxy-steam reforming of methanol. Applied Catalysis B: Environmental 2016;185:281-94.
[33] Singha RK, Yadav A, Agrawal A, Shukla A, Adak S, Sasaki T, et al. Synthesis of highly coke resistant Ni nanoparticles supported MgO/ZnO catalyst for reforming of methane with carbon dioxide. Applied Catalysis B: Environmental 2016;191:165-78.
[34] Wu Y, Pei C, Tian H, Liu T, Zhang X, Chen S, et al. Role of Fe Species of Ni-Based Catalysts for Efficient Low-Temperature Ethanol Steam Reforming. JACS Au 2021;1(9):1459-70.
[35] Kuo M-T, Chen Y-Y, Hung W-Y, Lin S-F, Lin H-P, Hsu C-H, et al. Synthesis of mesoporous CuFe/silicates catalyst for methanol steam reforming. International Journal of Hydrogen Energy 2019;44(28):14416-23.
[36] Chao P-Y, Hsu C-H, Lin H-P. Template-free synthesis of mesoporous Mn3O4-Al2O3 catalyst for low temperature selective catalytic reduction of NO with NH3. Journal of the Taiwan Institute of Chemical Engineers 2019;96:627-33.
[37] Kacker RN, Lagergren ES, Filliben JJ. Taguchi's Orthogonal Arrays Are Classical Designs of Experiments. J Res Natl Inst Stand Technol 1991;96(5):577-91.
[38] Canel T, Kaya AU, Çelik B. Parameter optimization of nanosecond laser for microdrilling on PVC by Taguchi method. Optics & Laser Technology 2012;44(8):2347-53.
[39] Chen W-H, Chen C-J, Hung C-I. Taguchi approach for co-gasification optimization of torrefied biomass and coal. Bioresour Technol 2013;144:615-22.
[40] Wang Y, Chen G, Li Y, Yan B, Pan D. Experimental study of the bio-oil production from sewage sludge by supercritical conversion process. Waste Manage 2013;33(11):2408-15.
[41] Chen W-H, Lin Y-Y, Liu H-C, Baroutian S. Optimization of food waste hydrothermal liquefaction by a two-step process in association with a double analysis. Energy 2020;199:117438.

[42] Lix LM, Keselman JC, Keselman HJ. Consequences of Assumption Violations Revisited: A Quantitative Review of Alternatives to the One-Way Analysis of Variance F Test. Review of Educational Research 1996;66(4):579-619.

[43] Parma A, Freris I, Riello P, Cristofori D, de Julián Fernández C, Amendola V, et al. Structural and magnetic properties of mesoporous SiO2 nanoparticles impregnated with iron oxide or cobalt-iron oxide nanocrystals. Journal of Materials Chemistry 2012;22(36):19276-88.

[44] Bahmanpour AM, Le Monnier BP, Du Y-P, Héroguel F, Luterbacher JS, Kröcher O. Increasing the activity of the Cu/CuAl2O4/Al2O3 catalyst for the RWGS through preserving the Cu2+ ions. Chemical Communications 2021;57(9):1153-6.

[45] Kunthakudee N, Khemthong P, Luadthong C, Panpranot J, Mekasuwandumrong O, Witoon T, et al. CuAl2O4–CuO–Al2O3 catalysts prepared by flame-spray pyrolysis for glycerol hydrogenolysis. Molecular Catalysis 2022;523:111426.

[46] Knox K. Le Châtelier's Principle. Journal of Chemical Education 1985;62(10):863.

[47] Liu Z, Chu B, Zhai X, Jin Y, Cheng Y. Total methanation of syngas to synthetic natural gas over Ni catalyst in a micro-channel reactor. Fuel 2012;95:599-605.

[48] Chen W-H, Shen C-T, Lin B-J, Liu S-C. Hydrogen production from methanol partial oxidation over Pt/Al2O3 catalyst with low Pt content. Energy 2015;88:399-407.

[49] Buckless FA, Ravenscroft SP. Contrast Coding: A Refinement of ANOVA in Behavioral Analysis. The Accounting Review 1990;65(4):933-45.

[50] Mosayebi A, Eghbal Ahmadi MH. Combined steam and dry reforming of methanol over Fe-Mn-Cu/ZrO2 catalyst to syngas formation: Study about kinetic and fuzzy model approaches. International Journal of Energy Research 2021;45(9):13878-96.

[51] Fajín JLC, Cordeiro MNDS. Insights into the Mechanism of Methanol Steam Reforming for Hydrogen Production over Ni–Cu-Based Catalysts. ACS Catalysis 2022;12(1):512-26.

[52] Ferreiro JP, Wilson M, Vázquez EV. Multifractal Description of Nitrogen Adsorption Isotherms. Vadose Zone Journal 2009;8(1):209-19.

[53] Buttersack C. Modeling of type IV and V sigmoidal adsorption isotherms. Physical Chemistry Chemical Physics 2019;21(10):5614-26.

[54] Abrokwah RY, Deshmane VG, Kuila D. Comparative performance of M-MCM-41 (M: Cu, Co, Ni, Pd, Zn and Sn) catalysts for steam reforming of methanol. Journal of Molecular Catalysis A: Chemical 2016;425:10-20.

[55] Bossola F, Roongcharoen T, Coduri M, Evangelisti C, Somodi F, Sementa L, et al. Discovering indium as hydrogen production booster for a Cu/SiO2 catalyst in steam reforming of methanol. Applied Catalysis B: Environmental 2021;297:120398.

[56] Zeng D, Pan M, Wang L, Tang Y. Fabrication and characteristics of cube-post microreactors for methanol steam reforming. Applied Energy 2012;91(1):208-13.

[57] Kundu A, Park JM, Ahn JE, Park SS, Shul YG, Han HS. Micro-channel reactor for steam reforming of methanol. Fuel 2007;86(9):1331-6.

[58] Yang H-M, Liao P-H. Preparation and activity of Cu/ZnO-CNTs nano-catalyst on steam reforming of methanol. Applied Catalysis A: General 2007;317(2):226-33.

[59] Tonelli F, Gorriz O, Tarditi A, Cornaglia L, Arrúa L, Cristina Abello M. Activity and stability of a CuO/CeO2 catalyst for methanol steam reforming. International Journal of Hydrogen Energy 2015;40(39):13379-87.

[60] Tajrishi OZ, Taghizadeh M, Kiadehi AD. Methanol steam reforming in a microchannel reactor by Zn-, Ce- and Zr- modified mesoporous Cu/SBA-15 nanocatalyst. International Journal of Hydrogen Energy 2018;43(31):14103-20.

[61] Lytkina AA, Zhilyaeva NA, Ermilova MM, Orekhova NV, Yaroslavtsev AB. Influence of the support structure and composition of Ni–Cu-based catalysts on hydrogen production by methanol steam reforming. International Journal of Hydrogen Energy 2015;40(31):9677-84.

[62] Tahay P, Khani Y, Jabari M, Bahadoran F, Safari N. Highly porous monolith/TiO2 supported Cu, Cu-Ni, Ru, and Pt catalysts in methanol steam reforming process for H2 generation. Applied Catalysis A: General 2018;554:44-53.

[63] Khzouz M, Gkanas EI, Du S, Wood J. Catalytic performance of Ni-Cu/Al2O3 for effective syngas production by methanol steam reforming. Fuel 2018;232:672-83.

[64] Kim W, Mohaideen KK, Seo DJ, Yoon WL. Methanol-steam reforming reaction over Cu-Al-based catalysts derived from layered double hydroxides. International Journal of Hydrogen Energy 2017;42(4):2081-7.

[65] Khzouz M, Wood J, Pollet B, Bujalski W. Characterization and activity test of commercial Ni/Al2O3, Cu/ZnO/Al2O3 and prepared Ni–Cu/Al2O3 catalysts for

hydrogen production from methane and methanol fuels. International Journal of Hydrogen Energy 2013;38(3):1664-75.

[66] De Rogatis L, Montini T, Lorenzut B, Fornasiero P. NixCuy/Al2O3 based catalysts for hydrogen production. Energy & Environmental Science 2008;1(4):501-9.

[67] Deshmane VG, Abrokwah RY, Kuila D. Synthesis of stable Cu-MCM-41 nanocatalysts for H2 production with high selectivity via steam reforming of methanol. International Journal of Hydrogen Energy 2015;40(33):10439-52.

611 **Table 1**

612 Operating factors and levels for the Taguchi method.

Factor		Level		
		1	**2**	**3**
A	Ni-Cu catalysts	10%	20%	30%
B	Reacting temperature (°C)	250	300	200
C	Flow rate of the carrier gas (N_2, $mL \cdot min^{-1}$)	1,000	1,500	2,000

613

614

Table 2

The Taguchi orthogonal array of L9 (3^3) at S/C= (a) 1.5 and (b) 2.0.

(a)

Case	S/C	Factor		
		A	B	C
1	1.5	1	1	1
2	1.5	1	2	2
3	1.5	1	3	3
4	1.5	2	1	2
5	1.5	2	2	3
6	1.5	2	3	1
7	1.5	3	1	3
8	1.5	3	2	1
9	1.5	3	3	2

(b)

Case	S/C	Factor		
		A	B	C
10	2.0	1	1	1
11	2.0	1	2	2
12	2.0	1	3	3
13	2.0	2	1	2
14	2.0	2	2	3
15	2.0	2	3	1
16	2.0	3	1	3
17	2.0	3	2	1
18	2.0	3	3	2

621 **Table 3**

622 MSR operating conditions and outcomes in the orthogonal arrays of the Taguchi method

Case	Conditions			MSR outcomes						
	Steam/Carbon ratio (S/C)	Ni-Cu cat. (%)	Reacting temp. (°C)	N_2 rate ($mL \cdot min^{-1}$)	H_2 (%)	CO_2 (%)	CO (%)	CH_4 (ppm)	CH_3OH conversion (%)	H_2 yield ($mol \cdot mol\ CH_3OH^{-1}$)
1	1.5	10	250	1,000	37.69	11.9	2.5	1,522	88.85	2.52
2	1.5	10	300	1,500	27.12	7.9	3.5	312	83.42	2.12
3	1.5	10	200	2,000	24.22	7.0	2.0	18	75.25	2.25
4	1.5	20	250	1,500	29.55	7.2	4.2	1,627	80.27	2.21
5	1.5	20	300	2,000	30.09	6.3	3.7	768	92.58	2.75
6	1.5	20	200	1,000	38.23	11.7	2.3	237	80.16	2.36
7	1.5	30	250	2,000	24.57	5.2	4.3	239	94.79	2.36
8	1.5	30	300	1,000	39.74	9.8	5.2	3,766	100.00	2.93
9	1.5	30	200	1,500	25.35	7.3	1.9	458	59.33	1.77
10	2.0	10	250	1,000	36.99	12.4	2.4	1,312	96.90	2.72
11	2.0	10	300	1,500	26.27	7.2	2.2	214	65.02	1.93
12	2.0	10	200	2,000	16.43	4.8	0.3	375	40.23	1.19
13	2.0	20	250	1,500	29.06	7.4	4.0	743	94.51	2.56
14	2.0	20	300	2,000	24.67	6.7	2.9	1,217	99.17	2.88
15	2.0	20	200	1,000	36.96	10.0	1.6	1,129	64.73	1.92
16	2.0	30	250	2,000	22.80	6.3	3.1	207	100.00	2.41
17	2.0	30	300	1,000	38.58	9.5	4.9	2,081	96.89	2.77
18	2.0	30	200	1,500	27.44	7.12	2.4	458	63.09	1.87

623

Table 4

Hydrogen yield and S/N in the Taguchi method at S/C= (a) 1.5 and (b) 2.0.

(a)

Case	Factor			H_2 yield (mol·mol CH_3OH^{-1})	S/N
	A	B	C		
1	1	1	1	2.52	8.03
2	1	2	2	2.12	6.53
3	1	3	3	2.25	7.04
4	2	1	2	2.21	6.89
5	2	2	3	2.75	8.79
6	2	3	1	2.36	7.46
7	3	1	3	2.36	7.46
8	3	2	1	2.93	9.34
9	3	3	2	1.77	4.96

(b)

Case	Factor			H_2 yield (mol·mol CH_3OH^{-1})	S/N
	A	B	C		
10	1	1	1	2.72	8.69
11	1	2	2	1.93	5.71
12	1	3	3	1.19	1.51
13	2	1	2	2.56	8.16
14	2	2	3	2.88	9.19
15	2	3	1	1.92	5.67
16	3	1	3	2.41	7.64
17	3	2	1	2.77	8.85
18	3	3	2	1.87	5.44

Table 5

Analysis of variance (ANOVA) in terms of hydrogen yield at S/C= (a) 1.5 and (b) 2.0.

(a)

S/C	Level	Factor			
		A	B	C	
1.5	1	2.29	2.36	2.60	-
	2	2.44	2.60	2.03	-
	3	2.35	2.12	2.45	-
	Factor	**S_i**	***f***	**Deviation from mean sum of squares**	**F value**
	A	0.031	2	0.015	3.00
	B	0.336	2	0.168	32.24
	C	0.523	2	0.261	50.25
	Error	0.031	6	0.005	-

(b)

S/C	Level	Factor			
		A	B	C	
2.0	1	1.94	2.56	2.47	-
	2	2.45	2.52	2.12	-
	3	2.35	1.66	2.16	-
	Factor	**S_i**	***f***	**Deviation from mean sum of squares**	**F value**
	A	0.430	2	0.215	5.86
	B	1.568	2	0.784	21.38
	C	0.220	2	0.110	3.00
	Error	0.220	6	0.036	-

Table 6

Performance comparison of MSR between this work and the results of the literature.

Catalyst	Supporter	Temperature (°C)	CH_3OH conversion (%)	Selectivity or H_2 yield	Ref.
Cu,	MCM-41	200-350	53.9-82.3	100-99.5% [a]	[54]
Ni	MCM-41	200-350	13.3-45.1	100-99.9% [a]	
Cu	MCM-41	300	89.5	100% [a]	[67]
$CuIn_x$	SiO_2	220		100% [a]	[55]
Cu/Zn	Al/Zr	260-280	70.3	94.8-98.7% [a]	[56]
Cu/ZnO	Al_2O_3	290	99.3	75% [b]	[57]
Cu/ZnO-CNTs	-	320	-	83.9% [a]	[58]
CuO-CeO_2	-	260-300	63.5-73.1	100% [a]	[59]
Cu/ZnO/CeO_2	ZrO_2/SBA-15	300	95.2	94.6% [a]	[60]
Ni-Cu	TiO_2/monolith	225-300	83.8-92.6	-	[62]
$Ni_{(10\%)}$-$Cu_{(10\%)}$	Al_2O_3 (80%)	275-325	86.9-96.1	1.84-2.08 [c]	[63]
$Ni_{0.2}Cu_{0.55}Al_{0.25}$	Al	190-300	5-15	-	[64]
$Ni_{0.2}$-$Cu_{0.8}$,	ZrO_2	300	-	1.4 [c]	[61]
$Ni_{0.8}$-$Cu_{0.2}$				1.2 [c]	
Ni-Cu	Al_2O_3	300	98.7	-	[65]
Ni_x-Cu_y-Al	Al_2O_3	230	-	2.0 [c]	[66]
$Ni_{(10\text{-}30\%)}$-Cu	**Al_2O_3**	**200-300**	**40.23-100**	**1.42-2.93 [d]**	**This study**

[a] selectivity (%), [b] concentration (vol %), [c] mol/mol CH_3OH

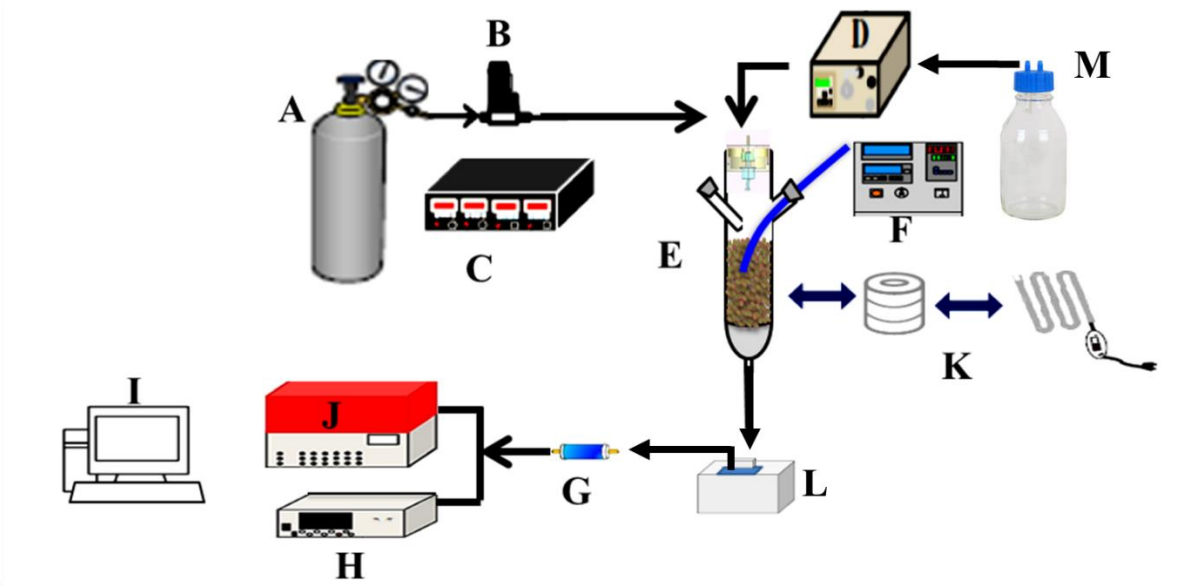

A: N_2 B: controller readout C: flow rate controller
D: pump E: reaction tube F: temperature monitor
G: drier H: gas analyzer I: recorder
J: GC K: refractory ceramic fiber L: condenser
M: methanol solution

639

640 **Fig. 1**. A schematic of the experimental system.

641

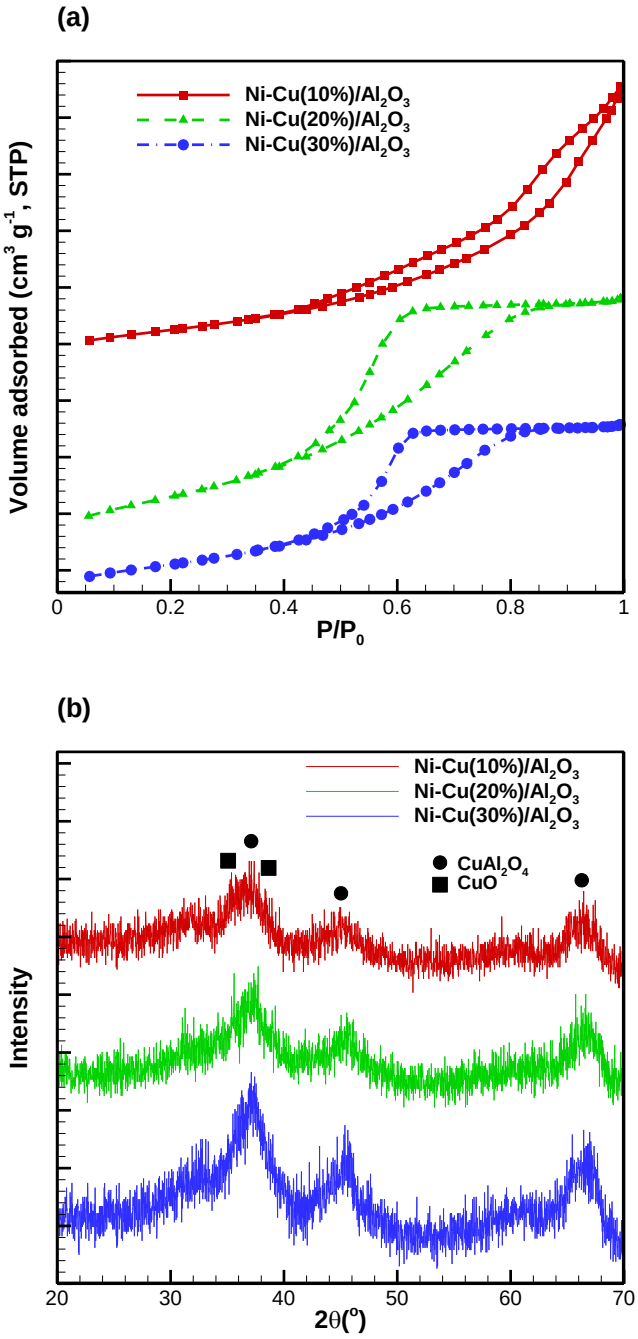

642

643 **Fig. 2**. (a) N_2 adsorption-desorption isotherms and (b) XRD patterns of three prepared Ni-

644 Cu/Al_2O_3 catalysts.

645

646

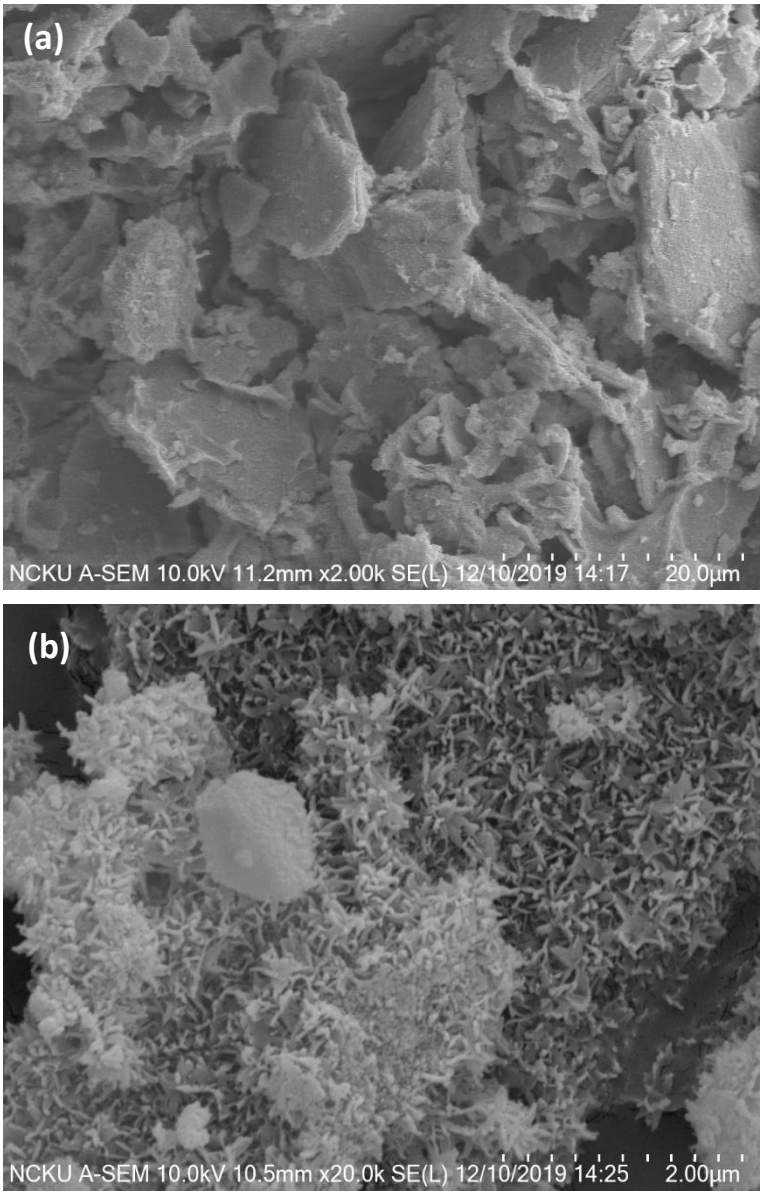

Fig. 3. SEM images of Ni-Cu(10%)/Al_2O_3 catalyst with magnifications of (a) 2,000 and (b) 20,000.

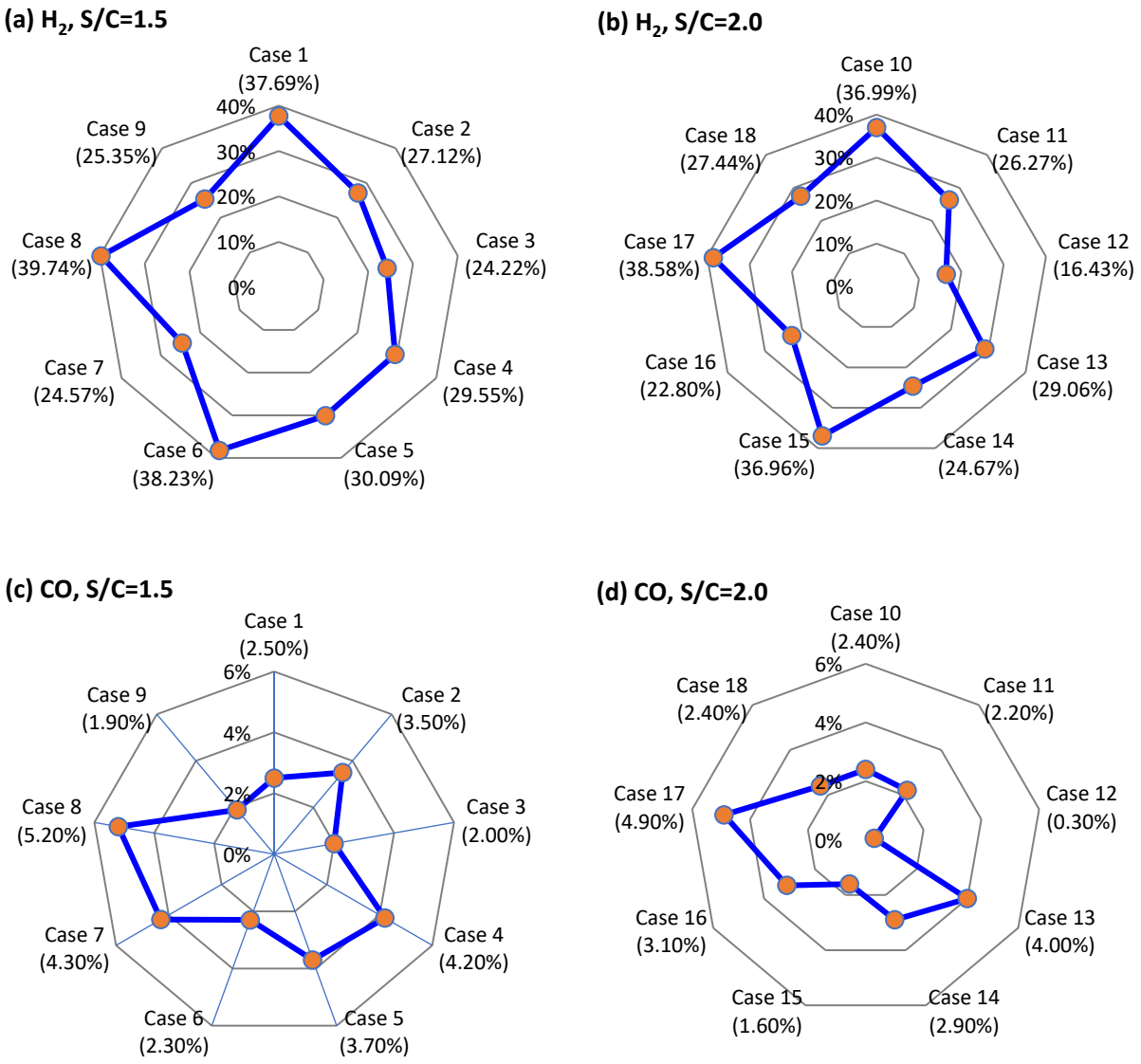

Fig. 4. The radar chars of H_2 concentration at S/C= (a) 1.5 and (b) 2.0 and CO concentration at S/C= (c) 1.5 and (d) 2.0.

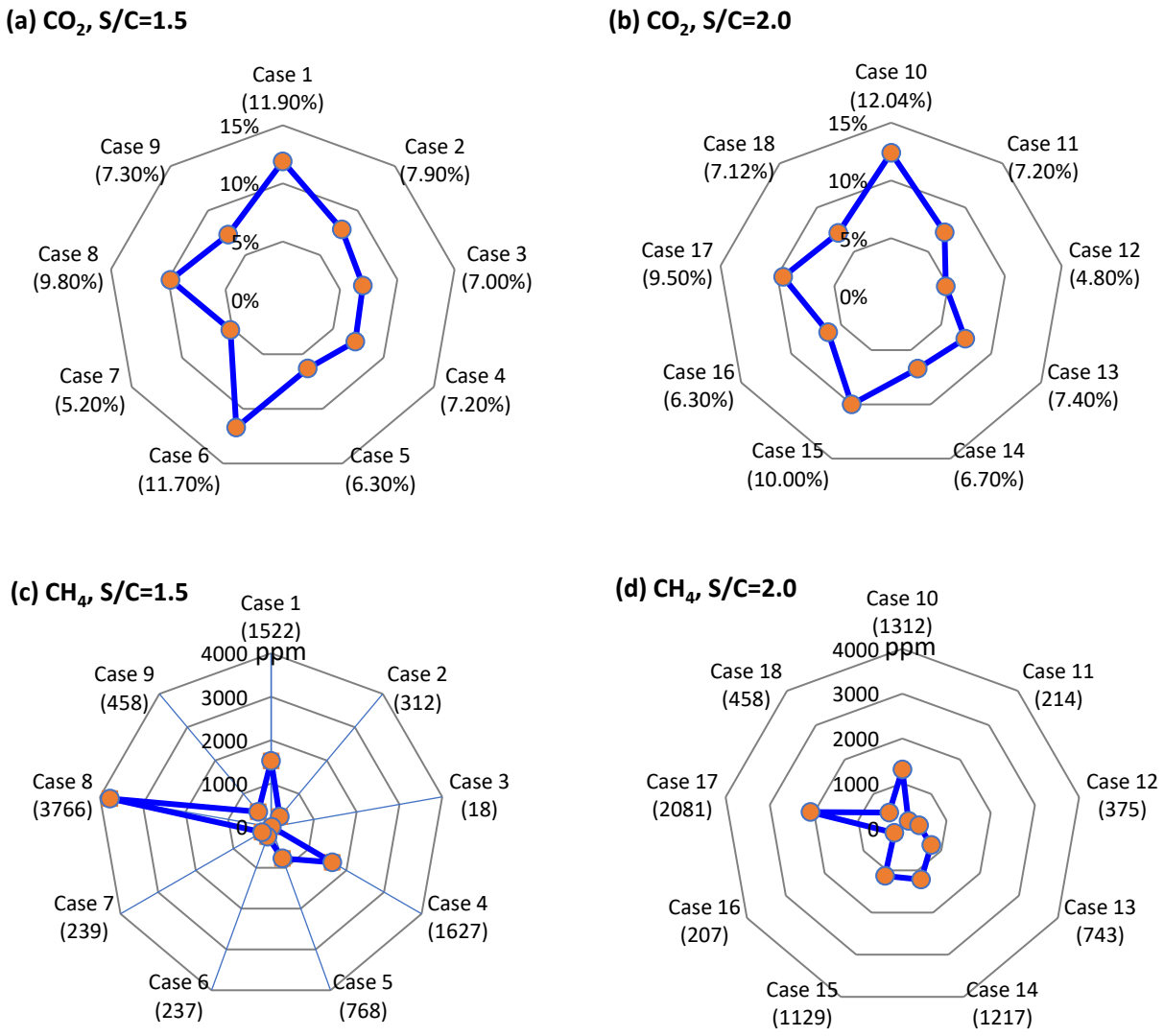

Fig. 5. The radar chars of CO_2 concentration at at S/C= (a) 1.5 and (b) 2.0 and CH_4 concentration at S/C= (c)1.5 and (d) 2.0.

661

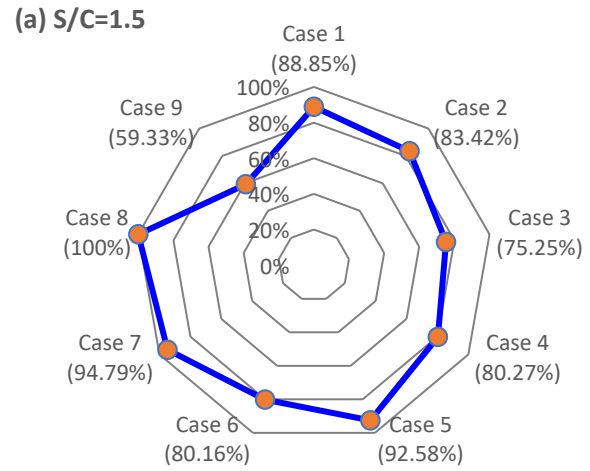

662

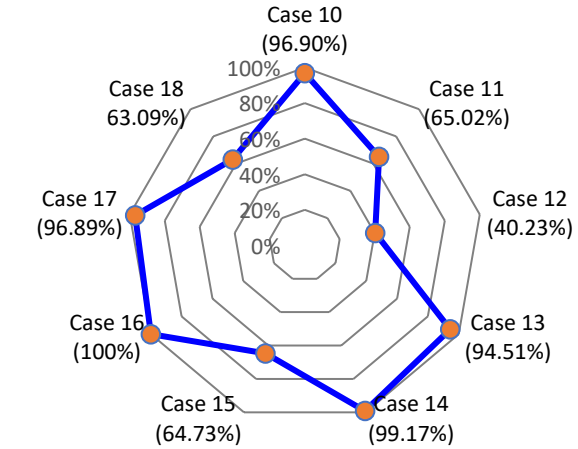

663 **Fig.6.** CH_3OH conversion radar charts at S/C= (a) 1.5 and (b) 2.0.

664

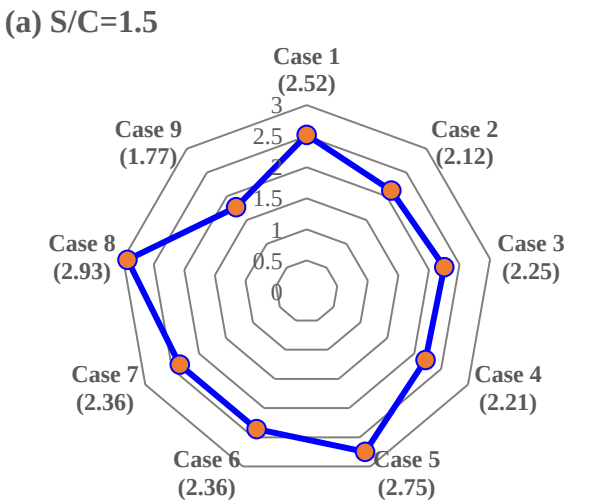

665

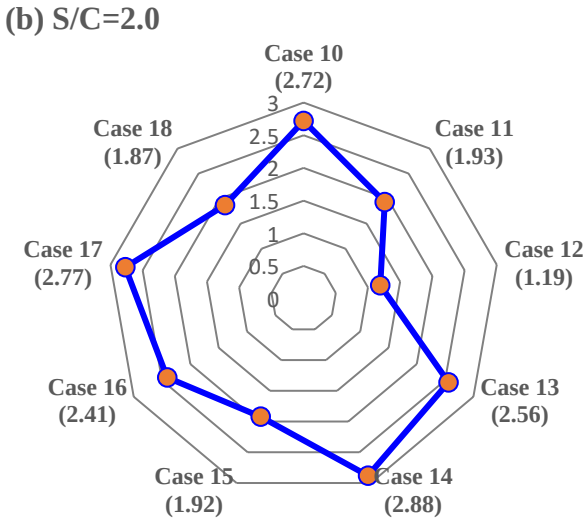

666

667 **Fig.7.** H_2 yield radar charts at S/C= (a) 1.5 and (b) 2.0.

668

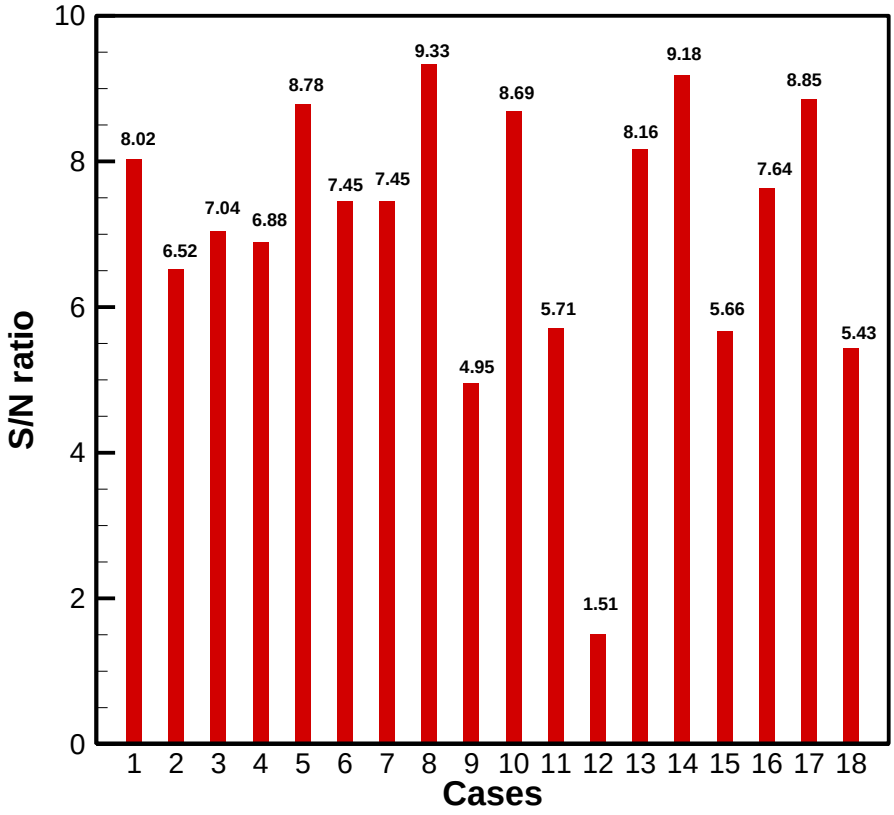

669

670 **Fig. 8**. S/N ratio profile of 18 cases in the Taguchi orthogonal arrays.

671

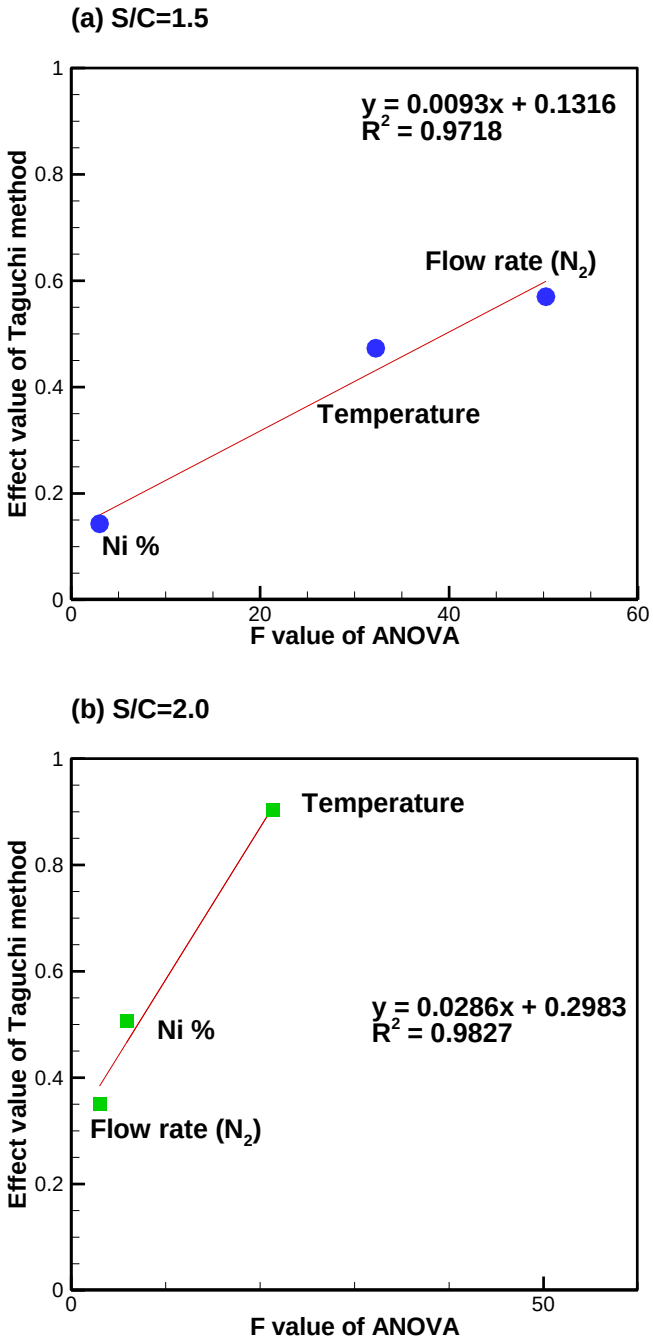

672

673 **Fig. 9.** Regression lines between the Taguchi effect value and ANOVA F value at S/C= (a) 1.5

674 and (b) 2.0.

675

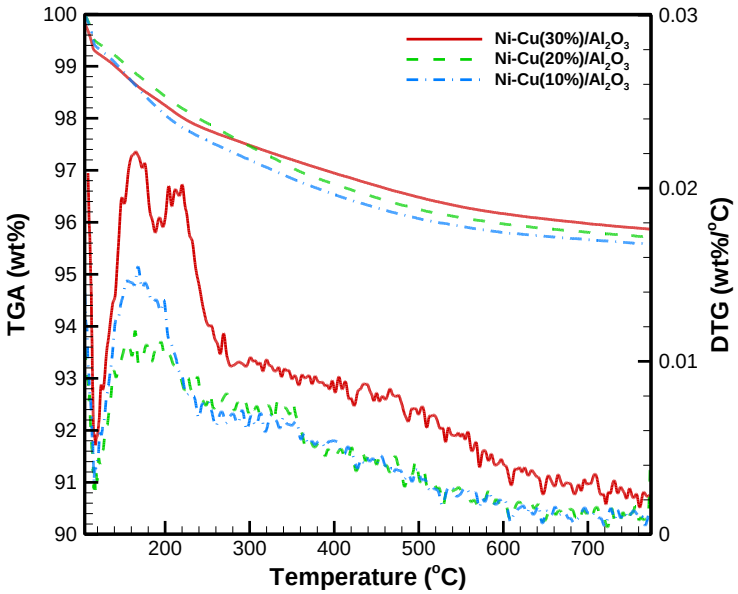

676

677 **Fig. 10.** Pyrolysis TGA and DTG curves of three catalysts at 20 °C·min^{-1} heating rate using O_2 as

678 a carrier gas.

679

680

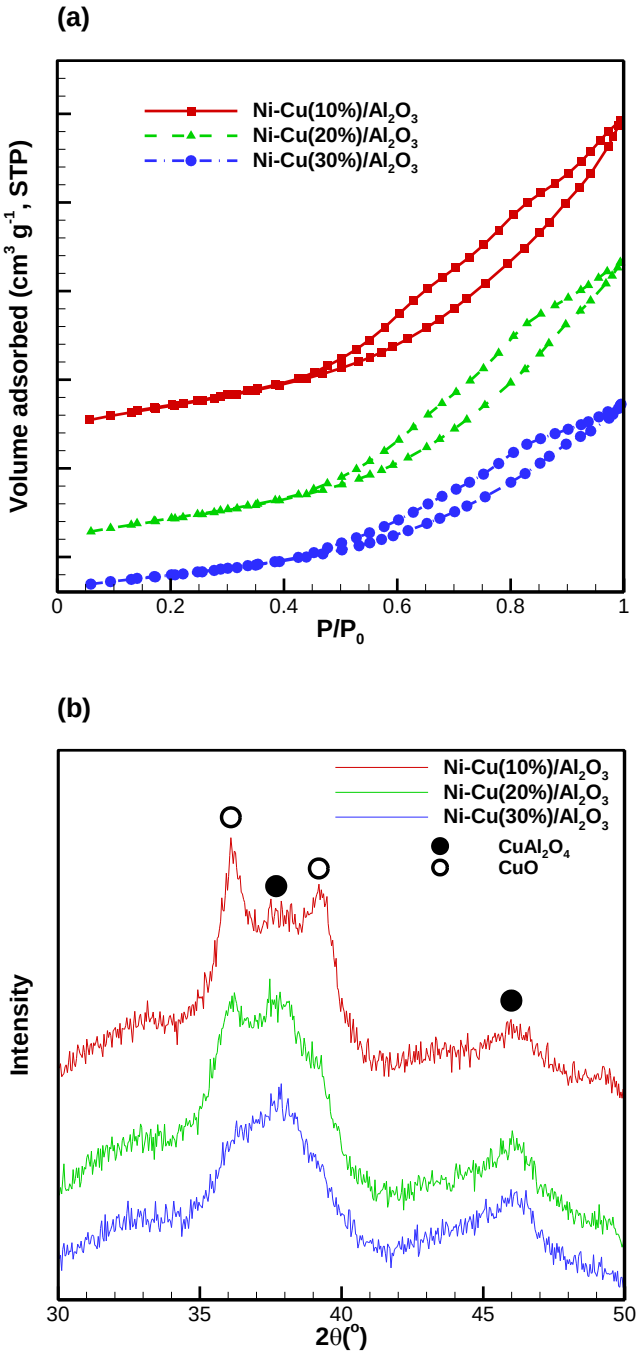

681

682 **Fig. 11.** (a) N_2 sorption isotherms and (b) XRD patterns for three recycled Ni-Cu/Al_2O_3 catalysts.

683

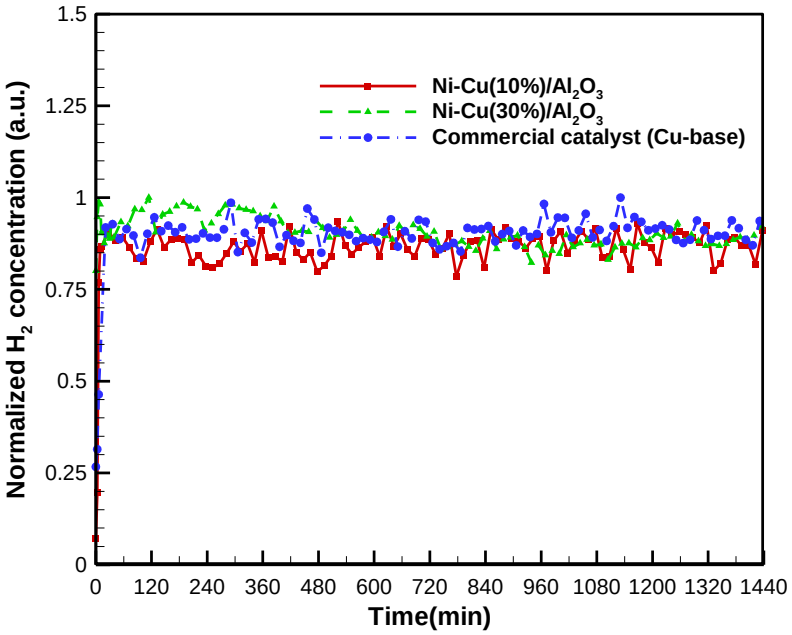

684

685 **Fig. 12.** Temporal profiles of hydrogen concentration in the long-term tests of three different

686 catalysts.

687

688